

# A Coarse-to-Fine Method for Infrared Small Target Detection

Shoukui Yao<sup>1</sup>, Yi Chang<sup>1</sup>, and Xiaojuan Qin<sup>1</sup>

**Abstract**—Infrared small target detection in a complex background is a challenging problem. A complex background generally contains structured edges, unstructured clutter, and noise, which completely have different properties. It is very difficult to separate small target from these interferences by exploiting one property. To solve this problem, we propose a coarse-to-fine method to gradually detect small target. In the coarse phase, nonlocal self-similarity property of the structured edges is exploited so as to separate the structured edges from the other components, such as the random noise, the unstructured clutter, and also the small target. In the fine phase, we utilize the local contrast prior of the small target in a local region so as to distinguish the small target from the unstructured clutter and noise. Multiscale information is further introduced to accommodate the changing size of the small target. This progressive detection pipeline utilizes the nonlocal, local, and multiscale information in a single image, which facilitates gradually differentiating the small target from the structured edges, unstructured clutter, and noise. Extensive experimental results demonstrate that the proposed method outperforms the state-of-the-art methods.

**Index Terms**—Coarse to fine (CF), infrared small target detection, local contrast, multiscale, nonlocal self-similarity.

## I. INTRODUCTION

**B**ECAUSE of the long imaging distance, infrared small targets usually do not possess concrete shape and texture. Additionally, infrared small targets are usually buried in strong edges, heavy unstructured clutter, and noise, such as cloud background and sea-sky background [1]. Therefore, infrared small target detection is a difficult and challenging problem, especially with complex background.

Existing infrared small target detection methods can be roughly categorized into two classes: sequential detection methods [2]–[5] and single-frame detection methods [6]–[11]. In this letter, we are interested in the single-frame detection. Conventional single-frame detection methods can be further divided into two categories: local prior-based methods and nonlocal prior-based methods.

Manuscript received December 23, 2017; revised August 12, 2018; accepted September 17, 2018. Date of publication October 15, 2018; date of current version January 21, 2019. This work was supported in part by the projects of the National Natural Science Foundation of China under Grant 61571207 and Grant 61433007 and in part by the National Key Research and Development Program under Grant 2016YFF0101502. (Shoukui Yao and Yi Chang contributed equally to this work.) (Corresponding author: Yi Chang.)

The authors are with the National Key Laboratory of Science and Technology on Multispectral Information Processing, School of Automation, Huazhong University of Science and Technology, Wuhan, China (e-mail: yichang@hust.edu.cn).

This paper has supplementary downloadable material available at <http://ieeexplore.ieee.org>, provided by the author.

Color versions of one or more of the figures in this letter are available online at <http://ieeexplore.ieee.org>.

Digital Object Identifier 10.1109/LGRS.2018.2872166

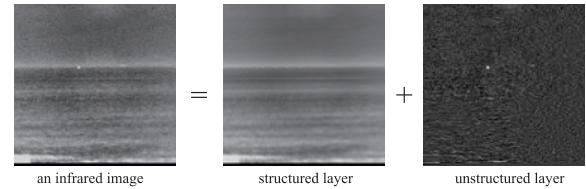


Fig. 1. Infrared image can be decomposed into a structured layer and an unstructured layer.

Local prior-based methods include filtering methods, such as top-hat filtering [8] and max-mean/max-median filtering [9], to name a few. Chen *et al.* [7] proposed the local contrast measure (LCM), which measured the dissimilarity between the current location and its neighborhood. Han *et al.* [10] proposed an improved LCM (ILCM), which further considered the mean estimation of the central subblock. However, these methods cannot separate small target with strong structured edges, because LCM is sensitive not only to small target but also to strong structured edges.

Gao *et al.* [6] formulated small target detection as an optimization problem of recovering low-rank and sparse matrices. This method effectively separated the structured edges from the sparse small target by exploiting the nonlocal self-similarity property. Bai *et al.* [11] exploited nonlocal self-similarity to estimate the background in infrared images for infrared small target detection. They have shown the effectiveness for structural edge modeling. However, the performance of these nonlocal prior-based methods degrades rapidly as the unstructured clutter and noise increase, because unstructured clutter and noise do not satisfy nonlocal self-similarity in the same way as the small target.

It is difficult to separate small target from complex background with just one prior. Therefore, we propose to combine the advantages of nonlocal and local prior and formulate the problem into a coarse-to-fine (CF) framework to gradually detect small target. In the coarse phase, we separate the structured edges from the small target, unstructured clutter, and noise by exploiting the nonlocal self-similarity in the image [12], [13]. To achieve this goal, an infrared image is decomposed into a structured layer and an unstructured layer. As shown in Fig. 1, the structured layer includes structured edges. The unstructured layer mainly contains small target, unstructured clutter, and noise. After the structured edges are removed, the small target appears distinct from the unstructured clutter and noise in the local zone. In the fine phase, we separate the small target from the unstructured clutter and noise in the unstructured layer by using the local prior. A multiscale modified LCM (MLCM) is proposed to

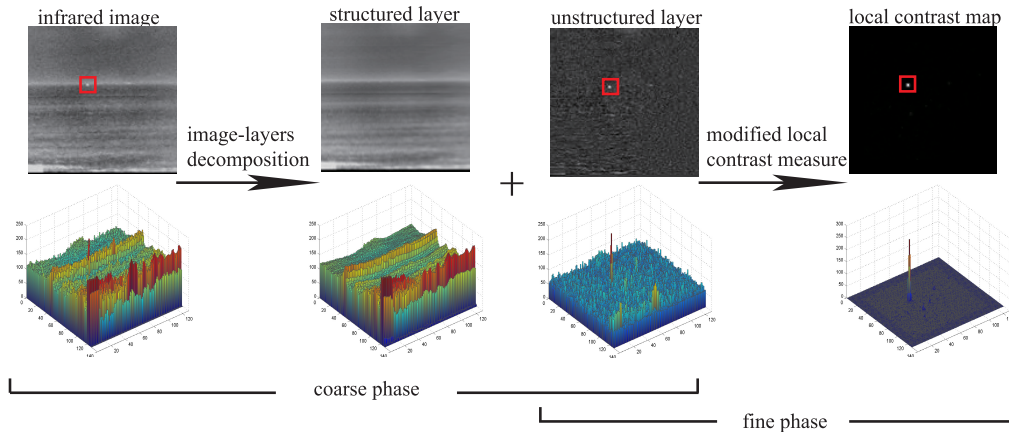


Fig. 2. Framework of our proposed method includes a coarse phase and a fine phase. In the coarse phase, an infrared image is decomposed into a structured layer and an unstructured layer via the low-rank decomposition. In the fine phase, small targets are distinguished from the unstructured clutter and noise. Targets are labeled by red boxes. First row: progressive detection procedure of the image. Second row: corresponding local contrast map.

distinguish the small target from the unstructured clutter and noise. The overall framework is shown in Fig. 2.

This letter is in line with the recently proposed reweighted infrared patch-tensor model [14]. The key insight of the two work is similar: both the nonlocal and local priors are benefit for the small target detection, and they are complementary to each other. As for the difference, in [14], they simultaneously utilize the local and nonlocal properties in the image and formulate the detection problem as an optimization problem in a unified framework. While in this letter, our philosophy is to decouple the complex problem into two simpler subproblems. Within such a CF pipeline, in each subproblem, we gradually obtain the small target. In addition, we take the multiscale operation into consideration for a better detection in the second stage.

The following contributions are made in this letter: 1) we propose to decompose a complicated problem into simple subproblems in which the small target is gradually extracted from the complex background; 2) we make use of the non-local, local, and multiscale information in a single image to gradually separate the small target from the structured edges, unstructured clutter, and noise; and 3) experimental results on several real image sequences demonstrated that our method outperforms the state-of-the-art methods.

## II. PROPOSED METHOD

It is difficult to separate the small target from complex background directly. Therefore, we propose to detect the small target with a CF process.

### A. Coarse Phase

The structural information in the infrared image usually has sharp edge and similar structural information among its local neighborhoods. While for the unstructured information, we mainly refer it as the random noise, the clutter, and also the small target, which exhibit singular characteristic in the infrared image. That is to say, we mainly utilize the self-similarity property of the infrared image to differ the structural (edge) from unstructured information (noise, clutter, and small target). To illustrate this, as shown in Fig. 2, we utilize the

structural self-similarity property of the infrared image by applying the low-rank decomposition. We can observe that an infrared image (first row, first image) can be well decoupled into two images: one mainly with structured edges (first row, second image) and one mainly with unstructured clutter and small target (first row, third image). This result is very reasonable. Structured edges possess nonlocal self-similarity property, while the unstructured clutter, the noise, and the small targets have sparse/singular property. Thus, we consider the edges in the infrared image as a structured layer and regard the other part of the infrared image as an unstructured layer. In the coarse phase, we separate the structured layer by exploiting the nonlocal self-similarity property in the coarse phase and then go one step further in the fine phase. We mathematically formulate the image decomposition as follows:

$$\mathbf{A} = \mathbf{U} + \mathbf{E} \quad (1)$$

where  $\mathbf{A}$  is an infrared image,  $\mathbf{U}$  is the structured layer, and  $\mathbf{E}$  is the unstructured layer.  $\mathbf{U}$  is a low-rank matrix for the structured layer that contains the nonlocal self-similarity

$$\text{rank}(\mathbf{U}) \leq \eta \quad (2)$$

where  $\eta$  is a constant. As the background becomes more complex, the value of  $\eta$  will increase. The unstructured layer  $\mathbf{E}$  includes small target, unstructured clutter, and noise. In general, the variance of the unstructured layer is limited

$$\|\mathbf{E}\|_1 \leq \delta \quad (3)$$

where  $\|\mathbf{E}\|_1 = \sum_{ij} |\mathbf{E}_{ij}|$  and  $\delta$  is a positive constant.

The decomposition problem can be solved by the robust principal component analysis [15]–[17]

$$\{\hat{\mathbf{U}}, \hat{\mathbf{E}}\} = \arg \min_{\mathbf{U}, \mathbf{E}} \|\mathbf{U}\|_* + \lambda \|\mathbf{E}\|_1, \quad \text{s.t. } \mathbf{A} = \mathbf{U} + \mathbf{E}. \quad (4)$$

This formula implicitly assumes that the structured layer is a single low-rank subspace. However, in most cases, the structured layer is drawn from a union of multiple subspaces. The decomposition may be inaccurate if the specifics of the multiple subspaces are not well defined. To better handle the

**Algorithm 1** Image-Layer Decomposition

- 
- 1: **input:** Infrared image  $A$ , parameter  $\lambda, \eta$ .
  - 2: **output:** Structured layer  $DZ$  and unstructured layer  $E$ .
  - 3: **initialization:**  $Z = J = 0, E = 0, Y_1 = 0, Y_2 = 0, \mu = 10^{-6}, \mu^{max} = 10^6, \rho = 1.1$ , and  $\varepsilon = 10^{-8}$ .
  - 4: **while** not converged **do**
  - 5:  $Z = J + \eta(D^T D)^{-1} D^T (A - E)$ ;
  - 6: Fix the others and update  $J$  by,
  - 7:  $J = \arg \min \frac{1}{\mu} \|J\|_* + \frac{1}{2} \|J - (Z + Y_2/\mu)\|_F^2$ ;
  - 8: Fix the others and update  $Z$  by,
  - 9:  $Z = (I + D^T D)^{-1} (D^T (A - E) + J + (D^T Y_1 - Y_2)/\mu)$ ;
  - 10: Fix the others and update  $E$  by,
  - 11:  $E = \arg \min \frac{\lambda}{\mu} \|E\|_1 + \frac{1}{2} \|E - (A - DZ + Y_1/\mu)\|_F^2$ ;
  - 12: Update the multipliers,
  - 13:  $Y_1 = Y_1 + \mu(A - DZ - E), Y_2 = Y_2 + \mu(Z - J)$ ;
  - 14: Update the parameter  $\mu$  by  $\mu = \min(\rho\mu, \mu^{max})$ ;
  - 15: Check the convergence conditions:
  - 16:  $\|A - DZ - E\|_\infty < \varepsilon$  and  $\|Z - J\|_\infty < \varepsilon$ .
  - 17: **end while**
- 

decomposition operation, we adopt the low-rank representation model to formulate the decomposition problem as

$$\{\hat{Z}, \hat{E}\} = \arg \min_{Z, E} \|Z\|_* + \lambda \|E\|_1, \quad \text{s.t. } A = DZ + E \quad (5)$$

where  $D$  is a ‘‘dictionary’’ that linearly spans the data space. After obtaining an optimal solution  $\hat{Z}$ , we obtain the structured layer by using  $D\hat{Z}$ . We adopt the augmented Lagrange multiplier (ALM) method [15], [18]. We first convert (5) to the following equation:

$$\{\hat{Z}, \hat{J}, \hat{E}\} = \arg \min_{Z, J, E} \|J\|_* + \lambda \|E\|_1 \quad \text{s.t. } A = DZ + E, \quad Z = J \quad (6)$$

where  $J$  is an auxiliary variable. The algorithm for solving the problem (6) by inexact ALM is shown in Algorithm 1. For simplicity, we set  $D$  as  $A$  similar to [19]. Lin *et al.* [18] demonstrated that Algorithm 1 has favorable convergence properties. It is worth noting that, to compensate the target that may be shrink by singular value shrink/threshold, we follow the iterative regularization [12], which can be regarded as an error retrieve strategy.

### B. Fine Phase

After the structured edges have been separated in the coarse phase, the small target is left in the unstructured layer together with the clutter and noise. In the fine phase, the multiscale MLCM based on the local prior is proposed to separate the small target from the clutter and noise. Assume  $w \in \mathbb{R}^2$  denotes the domain on which the unstructured layer  $E$  is defined.  $u$  and  $v$  denote pieces of the domain and satisfy  $u \subset v \subset w$ . Thus,  $E_u$  is a patch within patch  $E_v$ , and  $E_v$  is a patch within the image  $E_w$ . The relationship of  $u, v$ , and  $w$  is shown in Fig. 3(a). We define  $u$  and  $v$  to be squares. The side length of  $v$  is triple the side length of  $u$ . Nine neighboring uniform squares can be obtained by placing  $u$  on  $v$ . The nine uniform squares are shown in Fig. 3(b).  $u_0$  is the central cell.

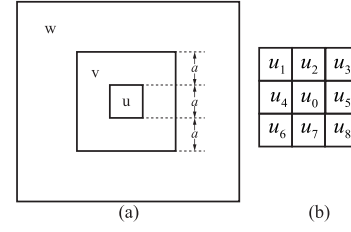


Fig. 3. (a) Relationship of domains  $u, v$ , and  $w$ . (b) Central cell  $u_0$  and the surrounding cells  $u_1 \sim u_8$ .

$u_1 \sim u_8$  are the surrounding cells. The LCM [7] is defined as

$$\text{LCM} = \min_i \frac{(L_f)^2}{m_i} \quad (7)$$

where  $L_f$  represents the first largest gray value of the central cell, and  $m_i$  represents the mean gray value of the  $i$ th surrounding cell. The central cell and surrounding cells are shown in Fig. 3(b). The LCM can effectively enhance the small targets and suppress background. However, the single-point noise would also be enhanced, while a homogeneous and less bright target would be weakened. To solve these problems, we propose to consider the second largest gray value of the central cell and the local similarity.

We present to replace  $(L_f)^2$  with  $L_f \times L_s$ , where  $L_s$  represents the second largest gray value of the central cell. Generally, the first and the second largest gray value of the true targets are nearly the same, while that are widely different in a cell containing strong single-point noise. The second largest gray value can enhance the true targets but not the single-point noise. We introduce  $|m_0 - m_i|$  to evaluate the local similarity between the central cell and the surrounding cells, where  $m_0$  is the mean gray value of the central cell. The local similarity reflects the difference of all of the pixels between the central cell and the surrounding cells. The local similarity can weaken the single-point noise and enhance the homogeneous and less bright targets. Thus, the MLCM is defined as

$$\text{MLCM} = \min_i \frac{|m_0 - m_i| \times L_f \times L_s}{m_i}, \quad i \in [1, 2, \dots, 8]. \quad (8)$$

When  $u_0$  is a small target, then  $m_0 > m_i$ ,  $L_f \approx L_s$ , and  $L_s > m_i$ , and the target will be enhanced. When  $u_0$  is a piece of unstructured clutter, then  $|m_0 - m_i| \approx 0$  and  $L_f \approx L_s \approx m_i$ , and the unstructured clutter will be suppressed. When  $u_0$  is a zone containing single-point noise with high brightness, then  $|m_0 - m_i| \approx 0$ ,  $L_f > L_s$ , and  $L_s \approx m_i$ , and the single-point noise will be suppressed.

The differences between MLCM and LCM are as follows. First, MLCM uses not only the largest gray value but also the second largest gray value of the central cell for suppressing the single-point noise. Second, MLCM exploits the local similarity to enhance the homogeneous and less bright small targets and further suppress the single-point noise. We calculate MLCM on a multiscale to accommodate the changing size of the small target, as shown in Algorithm 2.

We conduct an experiment to compare the MLCM with LCM [7] and ILCM [10]. An example of the results is shown in Fig. 4. Clearly, the MLCM outperforms all other contrast-based methods. Furthermore, we compare the results

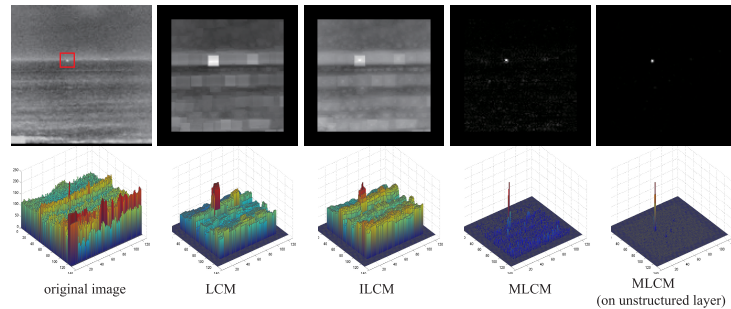


Fig. 4. Comparison of the local contrast maps calculated by different methods, including LCM, ILCM, and MLCM. It is clear that the MLCM outperforms the other local contrast-based methods. The MLCM on the unstructured layer outperforms that on original image. The target in the original image is labeled by red box.

---

**Algorithm 2** MLCM Computation
 

---

- 1: **input:** Unstructured layer  $E$ , patch-size  $l$ .
  - 2: **output:** Local contrast map  $M^l$ .
  - 3: Slip patch  $v$  on image  $E$  to get overlapped patches  $v_n$ ,  $n \in \{1, 2, \dots, N\}$ ;
  - 4: **for**  $n = 1 : N$  **do**
  - 5:   Slip patch  $u$  on patch  $v_n$  to get nine neighboring patches  $u_i$ ,  $i \in \{0, 1, \dots, 8\}$ ;
  - 6:   Compute the largest and the second largest value of the central cell,
  - 7:    $L_f = \max(I \in E_{u_0})$ ,  $L_s = \max(I \in E_{u_0} | I \neq L_f)$ ;
  - 8:   **for**  $i = 0 : 8$  **do**
  - 9:     Calculate the mean value,  $m_i = \frac{1}{N_{u_i}} \sum_{(j,t) \in u_i} E_{jt}$ ;
  - 10:   **end for**
  - 11:   Calculate the MLCM on patch  $u_0$  within  $v_n$ ,  $M_n^l = \min_i \frac{|m_0 - m_i| \times L_f \times L_s}{m_i}$ ,  $i \in [1, 2, \dots, 8]$ ;
  - 12: **end for**
- 

of MLCM on the original image and the unstructured layer. The results show that the MLCM performs better on the unstructured layer than that on the original image. This demonstrates that the extraction of the structured edges in the coarse phase is beneficial to the detection. More evidence to demonstrate the effectiveness of MLCM can be found in the Supplementary Material.

### III. EXPERIMENTS AND ANALYSIS

We compare the proposed CF algorithm with the infrared patch-image model-based method [6], the LCM [7], the ILCM [10], the top-hat method [8], and the max-mean/max-median method [9]. The codes of these algorithms are obtained from the websites of the authors, and the default parameter settings are used.

We have performed simulating experiments to evaluate the parameters for the method. In the coarse phase, the size of the sliding window is set as  $40 \times 40$ , and the size of the step is set as 7. In the fine phase, the size of the central patch  $u_0$  is set at  $3 \times 3$  and  $5 \times 5$  for the multiscale MLCM calculation. Due to the limited space of GRSL, we place the parameter analysis in the Supplementary Material.

In the experiments, we use the detection rate ( $R_d$ ) and false alarms ( $F_a$ ) per image sequence as standards for comparison.

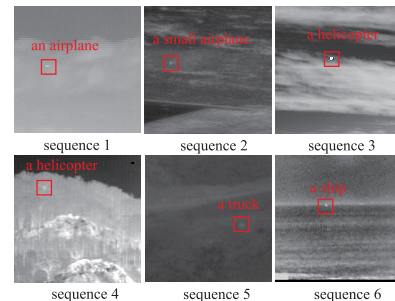


Fig. 5. All of the experimental image sequences have complex background and different clutters. The detailed description of the image sequences can be found in the Supplementary Material. The targets have been labeled by red boxes.

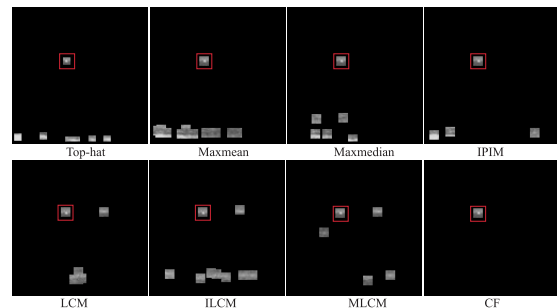


Fig. 6. Comparison of detection results of an example.

We define that  $R_d = (\text{CN}/\text{TN}) \times 100\%$  and  $F_a = \text{ICN}/\text{IN}$ , where CN is the number of correctly detected targets, TN is the number of true targets, ICN is the number of incorrectly detected targets, and IN is the number of images in the sequence. Experimental data sets are shown in Fig. 5. There are six real infrared image sequences.

The CF method succeeds in detecting the true target without any false alarms. While the competing methods identify the true target, there are still false alarms (see Fig. 6). The false alarms are clutter with high brightness, such as sea waves. It is clear that the CF method outperforms the competing methods for target detection in the representative images.

To further validate the generalization of the CF algorithm, we compare the probability of detection of the competing methods under several false-alarm rates. In Table I, the detection results on six infrared image sequences are shown. It is clear that the proposed CF method outperforms all of the other methods. The CF method has a higher probability of detection compared to the other methods when the false-alarm rates

TABLE I

DETECTION RESULTS OF OUR ALGORITHM COMPARED WITH THE OTHER METHODS ON SIX REAL INFRARED IMAGE SEQUENCES. IT IS SHOWN THAT OUR METHOD HAS THE HIGHEST PROBABILITY OF DETECTION COMPARED TO THE OTHER METHODS WHEN THE FALSE-ALARM RATES ARE LOW. THE BOLD NUMBER REPRESENTS THE HIGHEST PROBABILITY OF DETECTION UNDER THE CORRESPONDING FALSE-ALARM RATE

$F_a$	0.5	0.6	0.7	0.8	0.9	1	1.1	1.2	1.3	1.4	1.5	1.6	1.7	1.8	1.9	2
Maxmean	0.28	0.29	0.31	0.32	0.33	0.34	0.35	0.35	0.36	0.36	0.37	0.38	0.38	0.38	0.38	0.39
Maxmedian	0.20	0.22	0.23	0.25	0.26	0.27	0.27	0.28	0.30	0.30	0.31	0.32	0.32	0.32	0.33	0.33
Top-hat	0.19	0.20	0.21	0.22	0.22	0.22	0.23	0.23	0.23	0.24	0.25	0.25	0.25	0.26	0.26	0.26
ILCM	0.25	0.27	0.28	0.28	0.29	0.30	0.30	0.30	0.31	0.31	0.31	0.31	0.31	0.31	0.32	0.33
LCM	0.29	0.31	0.31	0.31	0.31	0.32	0.32	0.32	0.33	0.34	0.34	0.34	0.34	0.34	0.36	0.36
IPIM	0.35	0.39	0.42	0.42	0.43	0.43	0.43	0.43	0.44	0.44	0.44	0.45	0.45	0.45	0.45	0.45
MLCM	0.43	0.46	0.48	0.50	0.51	0.52	0.53	0.54	0.54	0.55	0.55	0.56	0.56	0.56	0.57	0.57
CF	<b>0.56</b>	<b>0.57</b>	<b>0.59</b>	<b>0.60</b>	<b>0.61</b>	<b>0.61</b>	<b>0.62</b>	<b>0.63</b>	<b>0.63</b>	<b>0.63</b>	<b>0.64</b>	<b>0.64</b>	<b>0.64</b>	<b>0.64</b>	<b>0.65</b>	<b>0.66</b>

are low. The results show that the proposed method is more stable for different complex backgrounds and target types.

The proposed method contains a coarse phase and a fine phase. In the coarse phase, the nonlocal self-similarity of the background is exploited to extract the sharp-structured edges. In the fine phase, the proposed multiscale MLCM is used to separate small targets from the other clutters and noise. Both the nonlocal and local priors along the multiscale prior are employed in a CF pipeline to gradually separate the small targets from the complex background. Comparing with the other sole-prior-based and sole-phase-based methods, our CF method performs better under complex background. We have also conducted the experiments on synthetic images to demonstrate the performance of the proposed method. The experimental results and analysis are placed in the Supplementary Material.

#### IV. CONCLUSION

In this letter, we propose a CF method for infrared small target detection. The key idea of infrared small target detection is to decouple the original problem into two easier sub-problems with clear physical meanings. In the coarse phase, the structured edges are removed by exploiting the nonlocal self-similarity prior. In the fine phase, the local prior-based multiscale MLCM is proposed to separate small target from unstructured clutter and noise. As a result, the small target is gradually separated and detected via the nonlocal prior, local prior, and multiscale information. Experimental results demonstrate that the proposed algorithm outperforms the state-of-the-art algorithms. In the future work, we would like to speed up the proposed method for real-time application.

#### ACKNOWLEDGMENT

The authors would also like to thank the handling editor and anonymous reviewers for their valuable remarks that greatly improve this work. The author, Shoukui Yao, would like to express his love to his girlfriend for supporting him extensively over his Ph.D., and ask his girlfriend to marry him.

#### REFERENCES

- [1] M. Malanowski and K. Kulpa, "Detection of moving targets with continuous-wave noise radar: Theory and measurements," *IEEE Trans. Geosci. Remote Sens.*, vol. 50, no. 9, pp. 3502–3509, Sep. 2012.
- [2] P.-L. Shui, D.-C. Li, and S.-W. Xu, "Tri-feature-based detection of floating small targets in sea clutter," *IEEE Trans. Aerosp. Electron. Syst.*, vol. 50, no. 2, pp. 1416–1430, Apr. 2014.
- [3] L. Dong, B. Wang, M. Zhao, and W. Xu, "Robust infrared maritime target detection based on visual attention and spatiotemporal filtering," *IEEE Trans. Geosci. Remote Sens.*, vol. 55, no. 5, pp. 3037–3050, May 2017.
- [4] Q. Wang, J. Wan, and Y. Yuan, "Locality constraint distance metric learning for traffic congestion detection," *Pattern Recognit.*, vol. 75, pp. 272–281, Mar. 2018.
- [5] Y. Yuan, Z. Xiong, and Q. Wang, "An incremental framework for video-based traffic sign detection, tracking, and recognition," *IEEE Trans. Intell. Transp. Syst.*, vol. 18, no. 7, pp. 1918–1929, Jul. 2016.
- [6] C. Gao, D. Meng, Y. Yang, Y. Wangm, X. Zhou, and A. G. Hauptmann, "Infrared patch-image model for small target detection in a single image," *IEEE Trans. Image Process.*, vol. 22, no. 12, pp. 4996–5009, Dec. 2013.
- [7] C. L. P. Chen, H. Li, Y. Wei, T. Xia, and Y. Y. Tang, "A local contrast method for small infrared target detection," *IEEE Trans. Geosci. Remote Sens.*, vol. 52, no. 1, pp. 574–581, Jan. 2014.
- [8] X. Bai and F. Zhou, "Analysis of new top-hat transformation and the application for infrared dim small target detection," *Pattern Recognit.*, vol. 43, no. 6, pp. 2145–2156, 2010.
- [9] S. D. Deshpande, M. H. Er, V. Ronda, and P. Chan, "Max-mean and max-median filters for detection of small-targets," *Proc. SPIE*, vol. 3809, pp. 74–83, Oct. 1999.
- [10] J. Han, Y. Ma, B. Zhou, F. Fan, K. Liang, and Y. Fang, "A robust infrared small target detection algorithm based on human visual system," *IEEE Geosci. Remote Sens. Lett.*, vol. 11, no. 12, pp. 2168–2172, Dec. 2014.
- [11] K. Bai, Y. Wang, and Q. Song, "Patch similarity based edge-preserving background estimation for single frame infrared small target detection," in *Proc. IEEE Int. Conf. Image Process.*, Sep. 2016, pp. 181–185.
- [12] Y. Chang, L. Yan, and S. Zhong, "Hyper-laplacian regularized unidirectional low-rank tensor recovery for multispectral image denoising," in *Proc. IEEE Conf. CVPR*, Jul. 2017, pp. 5901–5909.
- [13] Y. Chang, L. Yan, T. Wu, and S. Zhong, "Remote sensing image stripe noise removal: From image decomposition perspective," *IEEE Trans. Geosci. Remote Sens.*, vol. 54, no. 12, pp. 7018–7031, Dec. 2016.
- [14] Y. Dai and Y. Wu, "Reweighted infrared patch-tensor model with both nonlocal and local priors for single-frame small target detection," *IEEE J. Sel. Topics Appl. Earth Observ. Remote Sens.*, vol. 10, no. 8, pp. 3752–3767, Aug. 2017.
- [15] E. J. Candès, X. Li, Y. Ma, and J. Wright, "Robust principal component analysis?" *J. ACM*, vol. 58, no. 1, pp. 1–37, 2009.
- [16] Y. Chang, L. Yan, H. Fang, and H. Liu, "Simultaneous destriping and denoising for remote sensing images with unidirectional total variation and sparse representation," *IEEE Geosci. Remote Sens. Lett.*, vol. 11, no. 6, pp. 1051–1055, Jun. 2014.
- [17] Z. Huang, Y. Zhang, Q. Li, T. Zhang, N. Sang, and H. Hong, "Progressive dual-domain filter for enhancing and denoising optical remote-sensing images," *IEEE Geosci. Remote Sens. Lett.*, vol. 15, no. 5, pp. 759–763, May 2018.
- [18] Z. Lin, R. Liu, and Z. Su, "Linearized alternating direction method with adaptive penalty for low-rank representation," in *Proc. NIPS*, 2011, pp. 612–620.
- [19] G. Liu, Z. Lin, S. Yan, J. Sun, Y. Yu, and Y. Ma, "Robust recovery of subspace structures by low-rank representation," *IEEE Trans. Pattern Anal. Mach. Intell.*, vol. 35, no. 1, pp. 171–184, Jan. 2013.